

# Extensive excitatory network interactions shape temporal processing of communication signals in a model sensory system

Xiaofeng Ma,<sup>1</sup> Tsunehiko Kohashi,<sup>1,2</sup> and Bruce A. Carlson<sup>1</sup>

<sup>1</sup>Department of Biology, Washington University in St. Louis, St. Louis, Missouri; and <sup>2</sup>Division of Biological Science, Graduate School of Science, Nagoya University, Nagoya, Japan

Submitted 28 February 2013; accepted in final form 24 April 2013

**Ma X, Kohashi T, Carlson BA.** Extensive excitatory network interactions shape temporal processing of communication signals in a model sensory system. *J Neurophysiol* 110: 456–469, 2013. First published April 24, 2013; doi:10.1152/jn.00145.2013.—Many sensory brain regions are characterized by extensive local network interactions. However, we know relatively little about the contribution of this microcircuitry to sensory coding. Detailed analyses of neuronal microcircuitry are usually performed *in vitro*, whereas sensory processing is typically studied by recording from individual neurons *in vivo*. The electrosensory pathway of mormyrid fish provides a unique opportunity to link *in vitro* studies of synaptic physiology with *in vivo* studies of sensory processing. These fish communicate by actively varying the intervals between pulses of electricity. Within the mid-brain posterior extero-lateral nucleus (ELp), the temporal filtering of afferent spike trains establishes interval tuning by single neurons. We characterized pairwise neuronal connectivity among ELp neurons with dual whole cell recording in an *in vitro* whole brain preparation. We found a densely connected network in which single neurons influenced the responses of other neurons throughout the network. Similarly tuned neurons were more likely to share an excitatory synaptic connection than differently tuned neurons, and synaptic connections between similarly tuned neurons were stronger than connections between differently tuned neurons. We propose a general model for excitatory network interactions in which strong excitatory connections both reinforce and adjust tuning and weak excitatory connections make smaller modifications to tuning. The diversity of interval tuning observed among this population of neurons can be explained, in part, by each individual neuron receiving a different complement of local excitatory inputs.

microcircuit; paired recording; sensory processing; temporal coding; electric fish

THE CENTRAL PROCESSING of sensory information involves both extrinsic inputs to a network and local interactions among neurons in that network. The neuronal basis of sensory processing is typically studied either at the single-neuron level, through intracellular or extracellular recordings, or at the level of brain regions, through brain imaging. A better understanding of local network dynamics is necessary for understanding how the cellular and molecular properties of individual neurons give rise to emergent global patterns of activity that underlie perception and behavioral control (Grillner et al. 2005). However, it is technically challenging to relate neuronal microcircuitry to behaviorally relevant information processing. Synaptic connectivity in sensory microcircuits is often studied through simultaneous intracellular recordings from multiple neurons *in vitro* (Brown and Hestrin 2009; Fino and Yuste 2011; Kampa

et al. 2006; Perin et al. 2011; Song et al. 2005). However, it is difficult to determine the functional specificity of those connections because responses to sensory stimuli usually cannot be determined *in vitro*. Paired intracellular recordings *in vivo* can reveal correlated activity during sensory processing (Poulet and Petersen 2008), but these experiments are challenging to perform and allow for only limited experimental control. Imaging and multichannel extracellular recordings can be used to monitor correlated activity across large populations of neurons *in vivo* (Ahrens and Keller 2013; Kwan and Dan 2012; Szuts et al. 2011), but subthreshold network interactions are generally not detectable. Here we describe an *in vitro* whole brain preparation that allowed us to obtain paired intracellular recordings from neurons in an intact sensory microcircuit while controlling the timing of synaptic input to the circuit in behaviorally relevant ways.

Mormyrid fish generate an electric organ discharge (EOD) used for active sensing (von der Emde 1999) and communication (Carlson 2006). The relative timing of each EOD is highly variable, with interpulse intervals (IPIs) ranging from tens of milliseconds to seconds. Mormyrids actively vary IPIs during social interactions, with distinct IPI sequences associated with behavioral contexts such as aggression, submission, schooling, courtship, and territoriality (Arnegard and Carlson 2005; Carlson 2002a; Wong and Hopkins 2007). These signals are analyzed in a sensory pathway that is dedicated to electric communication behavior (Baker et al. 2013; Xu-Friedman and Hopkins 1999). The timing of each EOD is precisely encoded into the spike times of peripheral electroreceptors called knollenorgans, thereby encoding IPIs into sequences of interspike intervals (Hopkins and Bass 1981; Lyons-Warren et al. 2012). This information is relayed to the midbrain posterior extero-lateral nucleus (ELp), where temporal filtering of afferent spike trains establishes single-neuron IPI tuning (Carlson 2009). ELp neurons are diverse in their tuning (Carlson 2009), suggesting that each particular IPI is represented by the firing of a distinct population of cells. Thus temporal filtering in ELp converts a temporal code for electric communication signals into a population code (Baker et al. 2013).

Studying a sensory pathway that is specialized for a specific function makes it relatively straightforward to relate the physiology of cells and circuits to their role in information processing. Furthermore, the encoding of stimuli into precisely timed spike sequences makes it easy to recreate the synaptic input patterns that occur in an intact animal and study the processing of behaviorally relevant information in a reduced *in vitro* preparation (George et al. 2011). The whole brain preparation we describe here allowed us to obtain simultaneous recordings

Address for reprint requests and other correspondence: B. A. Carlson, Dept. of Biology, Campus Box 1137, Washington Univ., St. Louis, MO 63130-4899 (e-mail: carlson.bruce@wustl.edu).

from ELP neuron pairs, characterize their IPI tuning, determine their synaptic connectivity, and elucidate the role of microcircuitry in determining the IPI tuning of individual neurons. Our results reveal high degrees of excitatory network connectivity that shape the temporal filtering of sensory input and suggest that neuronal microcircuitry can contribute to the population coding of stimulus variation by establishing diverse response properties among a population of neurons.

## MATERIALS AND METHODS

**Animals.** We used both sexes of the mormyrid *Brienomyrus brachyistius* (Gill 1862), ranging from 1.2 to 9.0 g in body mass and from 5.0 to 9.5 cm in standard length. The fish were obtained through commercial vendors and housed in community tanks with a 12:12-h light-dark cycle, temperature of 25–28°C, pH of 6–7, and water conductivity of 200–400  $\mu\text{S}/\text{cm}$ . Fish were fed live black worms four times per week. All procedures were in accordance with guidelines established by the National Institutes of Health and were approved by the Animal Care and Use Committee at Washington University in St. Louis.

**Whole brain preparation.** We anesthetized fish in 100 mg/l MS-222 and then submerged fish in ice-cold, oxygenated artificial cerebrospinal fluid (ACSF; composition in mM: 124 NaCl, 2.0 KCl, 1.25  $\text{KH}_2\text{PO}_4$ , 24  $\text{NaHCO}_3$ , 2.6  $\text{CaCl}_2$ , 1.6  $\text{MgSO}_4 \cdot 7\text{H}_2\text{O}$ , and 20 glucose, pH 7.2–7.4; osmolarity 300–305 mosM) before performing a craniotomy to fully expose the brain. While the brain remained submerged, all cranial nerves were cut, the connection to the spinal cord was severed, and the valvula cerebellum was removed by suction, leaving the remaining hindbrain, midbrain, and forebrain intact (Fig. 1A). The brain was then removed and placed in an incubating chamber containing oxygenated ACSF at 29°C for 1 h. The brain was then transferred to a recording chamber (Warner Instruments RC-26GLP) that was continuously perfused with oxygenated ACSF at room temperature (flow rate = 1 ml/min), where it was placed on an elevated slice hold-down with a 1.0-mm mesh size (Warner Instruments SHD-26GH/10). A second slice hold-down with a 1.5-mm mesh size (Warner Instruments SHD-26GH/15) was placed on top of the brain, and it was held securely in place with cured silicone placed at the top of the chamber. Some of the threads of the upper hold-down were cut to improve access to the anterior and posterior extero-lateral nuclei (ELa and ELP, respectively). This configuration helped keep the preparation stable while also maximizing tissue survival by allowing a constant flow of oxygenated ACSF both beneath and above the preparation.

**Paired whole cell recording.** We visualized ELP neurons with transmitted light in an upright fixed-stage microscope (BX51WI; Olympus) in combination with a Newvicon tube camera (Dage-MTI). We obtained whole cell intracellular recordings with filamented borosilicate patch pipettes (1.00-mm outer diameter; 0.58-mm inner diameter) with tip resistances of 6.2–10.2  $\text{M}\Omega$  as described previously (George et al. 2011). The electrode internal solution contained the following (in mM): 130 K gluconate, 5 EGTA, 10 HEPES, 3 KCl, 2  $\text{MgCl}_2$ , 4  $\text{Na}_2\text{ATP}$ , 5  $\text{Na}_2$  phosphocreatine, and 0.4  $\text{Na}_2\text{GTP}$ , pH 7.3–7.4 (osmolarity: 285–290 mosM). Two electrodes were mounted in separate headstages (Molecular Devices CV-7B), both connected to a multichannel amplifier (Molecular Devices MultiClamp 700B) for two-channel current- or voltage-clamp recording (Fig. 1B). Data were digitized at a sampling rate of 50 kHz (Molecular Devices Digidata 1440A) and saved to disk (Molecular Devices Clampex v10.2). The position of each electrode was controlled by separate manipulators (Sutter Instruments MP-285), both connected to a single controller (Sutter Instruments MPC-200 and ROE-200). Healthy ELP neurons were identified on the basis of location and a relatively low-contrast, round somatic boundary. We targeted somas of all possible sizes and locations throughout ELP, but we were only able to see neurons located within  $\sim 20$ – $50 \mu\text{m}$  of the surface, depending on tissue

thickness. After both electrodes were placed near different somas, suction was applied to form a seal before breaking through the membrane, one neuron at a time. Seal resistance varied from 1.3 to 4.8  $\text{G}\Omega$ , and input resistance varied from 230 to 290  $\text{M}\Omega$ . We only used data from neurons that had stable access and input resistances and a stable resting potential of at least  $-40 \text{ mV}$ . We measured the inter-somatic distance between each recorded pair of neurons.

**Responses to afferent stimulation.** We placed an array of stimulus electrodes in ELa, just anterior to the ELP border (Fig. 1B). The array consisted of four channels of bipolar stimulation (8 electrodes total), in the form of either a “cluster” electrode (FHC model CE) or a “matrix” electrode (FHC model MX). We delivered simultaneous, isolated, biphasic, square current pulses with a total duration of 100  $\mu\text{s}$  and amplitudes ranging from 50 to 200  $\mu\text{A}$  through four separate isolated pulse generators (A-M Systems model 2100), each triggered by a single digital output (Molecular Devices Digidata 1440A). Stimulation on each channel was turned on or off, and stimulus amplitude was adjusted to yield reliable synaptic potentials from both recorded neurons. After setting the stimulus parameters, we stimulated ELa with single pulses as well as stimulus trains of 10 pulses with constant IPIs ranging from 10 to 100 ms while recording in current clamp, as described previously (George et al. 2011). Synaptic potentials were averaged across five repetitions of each stimulus. If there was any spiking, we applied a median filter to remove spikes before averaging (Carlson 2009; George et al. 2011).

We determined IPI tuning in response to constant-interval stimulus trains as described previously (Carlson 2009; George et al. 2011). We determined the resting potential as the average membrane potential within a 50-ms window during the prestimulus period. We measured the maximum depolarization in response to each stimulus pulse relative to rest and then averaged the maximum depolarizations in response to the 2nd through 10th pulses to quantify the response to each IPI; finally, we normalized these responses to the strongest response across IPIs. IPI tuning was categorized as all-pass, low-pass, high-pass, band-pass, band-stop, or complex with an 85% response criterion as described previously (Carlson 2009; George et al. 2011). In some cases in which one of the two cells spiked in response to ELa stimulation, we repeated this procedure while hyperpolarizing the spiking cell to approximately  $-90 \text{ mV}$  to prevent it from spiking. This allowed us to determine the effects of silencing the spiking cell on the IPI tuning of the second cell. Unless otherwise stated, all values are presented as means  $\pm$  SE.

**Characterization of synaptic connections.** We injected brief (2–3 ms) depolarizing current pulses (600 pA) in current clamp to elicit single, time-locked action potentials in one neuron while making current-clamp recordings from a second neuron. This was repeated 15 times to determine whether any postsynaptic potentials (PSPs) were present in the second neuron, and then we repeated the same procedure in reverse by stimulating the second cell while recording from the first. Chemical excitatory synaptic connections were identified as depolarizing voltage changes beginning within 10 ms of the presynaptic action potential peak, with a consistent latency (within  $\pm 250 \mu\text{s}$ ) across all 15 repetitions, and in which the peak of the averaged potential occurred  $> 1 \text{ ms}$  after the presynaptic action potential peak and with an amplitude  $> 2$  standard deviations of the baseline potential. We also looked for inhibitory synaptic connections, using the same criteria to detect consistent hyperpolarizing voltage changes; however, we only detected two inhibitory connections, so we focused on excitatory synaptic connections in this study. Electrical synaptic connections were identified as changes in voltage that closely followed presynaptic action potential waveforms with no detectable latency (“spikelets”). In one case, a strong electrical synaptic connection was also evident as step changes in voltage in response to step current injection into the other neuron. In all other cases, however, the electrical synaptic connections were much weaker and were only detectable as spikelets after averaging.

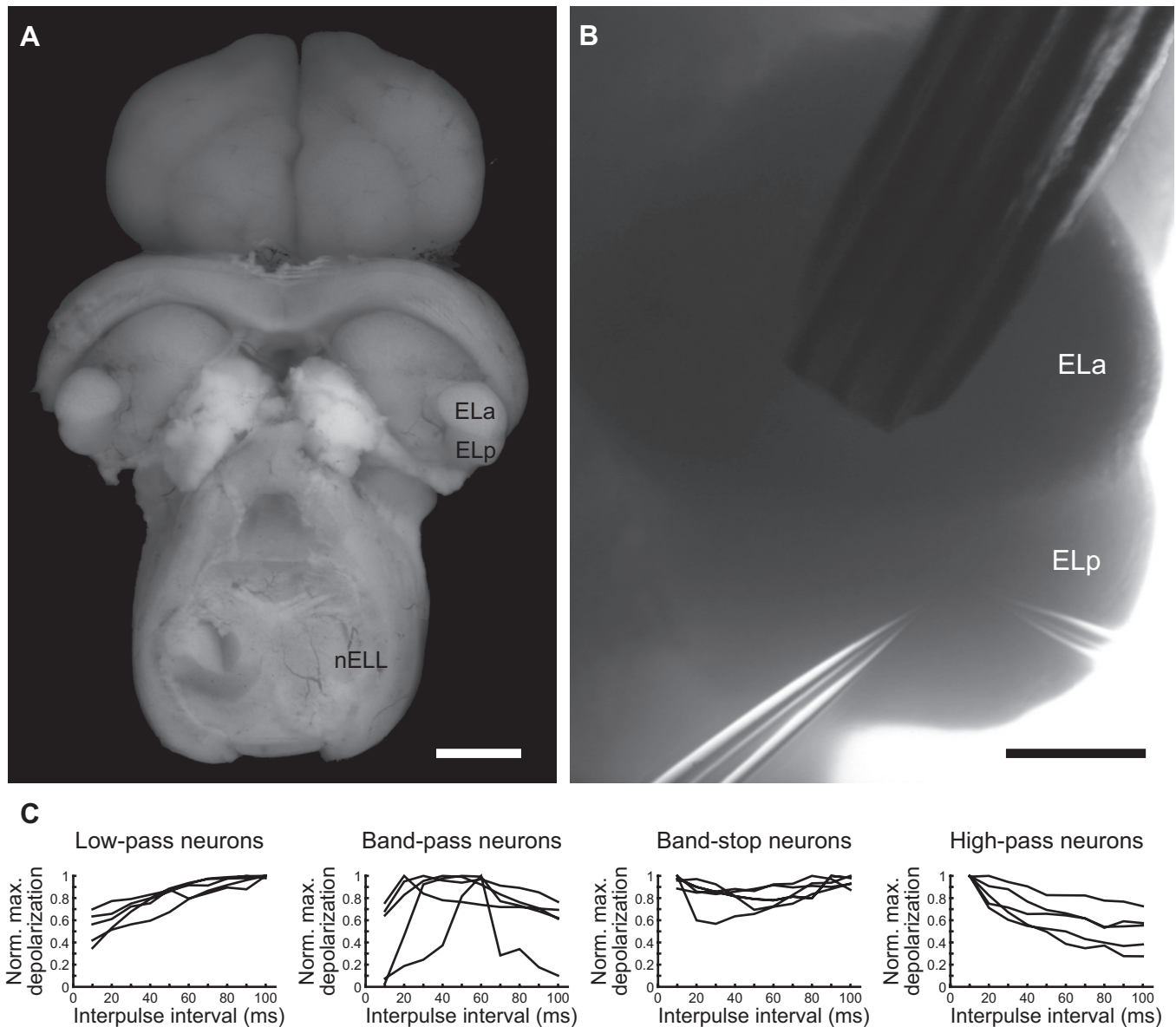


Fig. 1. Whole brain preparation and interpulse interval (IPI) tuning in posterior extero-lateral nucleus (ELp) neurons. *A*: dorsal view of the whole brain preparation, which consists of the entire brain except for the valvula cerebellum, which was removed by suction to expose the underlying hindbrain and midbrain. Primary afferents from knollenorgan electroreceptors terminate ipsilaterally in the hindbrain nucleus of the electrosensory lateral line lobe (nELL). Axons from nELL neurons project bilaterally to the midbrain anterior extero-lateral nucleus (ELA), which then projects to the adjacent ELp. Scale bar, 1 mm. *B*: close-up view of ELa and ELp during recording and stimulation. Electric stimuli are applied to ELa with a 4-bipolar-channel matrix electrode, which can be seen originating from the top right. Two patch pipettes are used for simultaneous whole cell recordings from pairs of ELp neurons. Scale bar, 200  $\mu\text{m}$ . *C*: tuning curves from 5 representative low-pass, band-pass, band-stop, and high-pass neurons. Curves show the average maximum depolarization in response to stimulation of ELa at IPIs ranging from 10 to 100 ms, normalized to the largest maximum depolarization of each unit.

If a synaptic connection was present, we sometimes delivered stimulus trains of 10 presynaptic spikes with constant intervals of 10, 50, and 100 ms. In each case, we delivered 15 repetitions of each stimulus and averaged across repetitions. We then measured the amplitude of excitatory postsynaptic potentials (EPSPs) or excitatory postsynaptic currents (EPSCs) relative to baseline, defined as the average membrane potential or holding current within a 50-ms window during the prestimulus period. We also measured the latency from presynaptic action potential peak to EPSP/EPSC peak (peak-to-peak latency) as well as the latency from presynaptic action potential peak to EPSP/EPSC onset, defined as the time at which the EPSP/EPSC reached 10% of the peak. Unless otherwise stated, all values are presented as means  $\pm$  SE.

**Pharmacology.** To assess the role of NMDA versus non-NMDA receptors in mediating glutamatergic EPSPs, we bath applied the NMDA receptor antagonist DL-2-amino-5-phosphonopentanoic acid (APV; Tocris 0105) and/or the non-NMDA receptor antagonist 6,7-dinitroquinoxaline-2,3-dione (DNQX; Tocris 2312). Both drugs were delivered at a concentration of 50  $\mu\text{M}$  in ACSF. Full washout typically took 15–20 min.

**Imaging physiologically identified neurons.** For visualizing synaptically connected neurons, we first identified a pair of connected neurons physiologically. We then applied slight positive pressure and slowly backed the recording electrodes away from the recorded neurons to minimize damage to the membranes. We then filled one electrode with 100  $\mu\text{M}$  Alexa Fluor 488 hydrazide (Life Technologies

A-10436) in internal solution and a second electrode with 100  $\mu\text{M}$  Alexa Fluor 568 hydrazide (Life Technologies A-10437) in internal solution. We then obtained patch recordings from the previously identified neurons with the dye-filled electrodes. After verifying the synaptic connection and holding the two cells at a stable resting potential for  $\sim 20$  min, we injected both cells with  $-20$  pA of hyperpolarizing current for 10–15 min to iontophoretically improve the label. We then applied slight positive pressure and slowly backed the recording electrodes away from the recorded neurons to minimize damage to the membranes. The tissue was then transported in oxygenated ACSF to a confocal fluorescence imaging setup consisting of an Olympus BX61 upright microscope and an FV1000 scanner. The tissue was continuously perfused with oxygenated ACSF during live imaging. Putative synaptic contacts were identified as close appositions between axonal boutons or axonal swellings of one neuron and the soma or dendrites of the second neuron in individual optical sections. Although this does not definitively identify functional synapses, electron microscopy has shown that a majority ( $\sim 80\%$ ) of such putative synapses represent actual functional synapses (Feldmeyer et al. 2002, 2006; Lübke et al. 1996; Markram et al. 1997; Mishchenko et al. 2010; Wang et al. 2002).

We also viewed neurons filled with biocytin obtained during *in vivo* recordings from ELP neurons in previous studies (see Carlson 2009; George et al. 2011). Briefly, we iontophoretically injected biocytin, using a 1-Hz sinusoidal current varying from 0 to +1 nA for 2–10 min, anesthetized fish in MS-222, and then perfused fish through the heart with ice-cold heparinized Hickman's Ringer solution followed by ice-cold 4% paraformaldehyde. After 3 h of postfixation, we embedded brains in gelatin, followed by an additional 3 h of postfixation. We cut 50- $\mu\text{m}$  horizontal sections with a vibratome, mounted the sections, and then used standard histological procedures to stain labeled cells (Carlson 2002b).

## RESULTS

Electrosensory input to ELP arises from the adjacent ELA (Fig. 1A). We classified the tuning of ELP neurons to IPI by delivering stimulus trains to ELA (Fig. 1B) and measuring the amplitude of PSP responses, as described previously (Carlson 2009; George et al. 2011). We recorded from all types of neurons encountered previously: "all-pass" neurons responded equally well to all IPIs between 10 and 100 ms; "low-pass" neurons responded preferentially to long IPIs; "high-pass" neurons responded preferentially to short IPIs; "band-pass" neurons responded preferentially to intermediate IPIs; "band-stop" neurons responded preferentially to both long and short, but not intermediate, IPIs; and "complex" neurons responded preferentially to multiple IPI ranges (Fig. 1C). The tuning of these cells to afferent stimulation patterns directly reflects the sensory coding of behaviorally relevant communication signals: individual ELP neurons respond similarly to sensory stimulation patterns and ELA microstimulation patterns *in vivo* (Carlson 2009), and for similarly tuned neurons the synaptic responses to sensory stimulation *in vivo* are similar to synaptic responses to afferent stimulation *in vitro* (George et al. 2011).

*Excitatory and electrical synaptic connections are widespread.* To identify and characterize synaptic connections among ELP neurons, we obtained dual whole cell recordings from a total of 407 neuron pairs. To test for synaptic connections, we injected brief (2–3 ms) depolarizing current pulses of sufficient amplitude (600 pA) to reliably elicit single spikes with high temporal precision in one neuron while recording under current clamp in the second neuron. Depolarizing EPSPs were clearly visible in 62 (15.2%) of these pairs (e.g., Fig. 2),

9 of which had a bidirectional excitatory connection, resulting in a total of 71 excitatory connections.

These EPSPs varied widely in amplitude from as small as 50  $\mu\text{V}$  to as large as 6.30 mV. Inward synaptic currents recorded while voltage-clamping postsynaptic cells at a holding potential of  $-60$  mV ranged from 2.47 to 61.05 pA ( $n = 15$ ). The distribution of synaptic strengths (EPSP amplitudes) was highly skewed [Lilliefors test:  $\text{KS}(71) = 0.23$ ,  $P < 0.001$ ], with the majority being relatively weak and a small number being relatively strong (Fig. 3A). A  $\log_{10}$ -transformation revealed that variation in synaptic strength followed a log-normal distribution (Fig. 3B) [ $\text{KS}(71) = 0.08$ ,  $P > 0.3$ ], as described for the distribution of synaptic strengths in cortical microcircuits (Song et al. 2005). The synaptic strengths of bidirectionally connected pairs were significantly larger than the synaptic strengths of unidirectionally connected pairs (Fig. 3C) [Mann-Whitney  $U$ -test:  $z(53,18) = 2.63$ ,  $P < 0.01$ ]. In addition, the synaptic strengths of bidirectionally connected pairs were strongly correlated with each other (Fig. 3D) (Spearman rank  $R = 0.85$ ;  $P < 0.01$ ). In only 1 of the 71 identified connections was the EPSP large enough to elicit spiking, and this only happened in 1 of the 15 stimulus repetitions. This strongly suggests that all observed postsynaptic responses were due to monosynaptic connections.

EPSP onset latencies averaged  $1.62 \pm 0.11$  ms (range: 0.41–5.47 ms), and peak-to-peak latencies averaged  $8.20 \pm 0.46$  ms (range: 1.30–25.20 ms). EPSC onset latencies averaged  $0.82 \pm 0.08$  ms (range: 0.33–1.57 ms), and peak-to-peak latencies averaged  $2.31 \pm 0.26$  ms (range: 1.34–4.90 ms). EPSP amplitude did not correlate with peak-to-peak latency (Spearman rank  $R = 0.02$ ;  $P > 0.8$ ), but it did negatively correlate with onset latency (Spearman rank  $R = -0.40$ ;  $P < 0.001$ ). Likewise, EPSC amplitude was negatively correlated with onset latency (Spearman rank  $R = -0.54$ ;  $P < 0.05$ ) but not peak-to-peak latency (Spearman rank  $R = -0.25$ ;  $P > 0.3$ ). This suggests that some of the variation in synaptic strength was due to the location of presynaptic terminals on dendritic arbors, with proximal inputs resulting in larger synaptic responses and shorter latencies at the soma compared with distal inputs.

We were able to visualize two pairs of synaptically connected neurons and identify potential synaptic contacts by filling recorded cells with Alexa Fluor dyes followed by confocal imaging of live tissue (Fig. 2). The morphology of the labeled cells was consistent with previous descriptions of ELP neuron morphology based on fixed tissue (George et al. 2011; Xu-Friedman and Hopkins 1999), including extensive dendritic arbors with visible spines as well as widely projecting axons giving rise to numerous collaterals. The excitatory synaptic connection of one of these pairs was relatively weak (349- $\mu\text{V}$  EPSP) and unidirectional (Fig. 2A). Putative synaptic contacts between axon collaterals of the presynaptic neuron and dendrites of the postsynaptic neuron were visible at two distinct locations (Fig. 2A). The other pair had a stronger, bidirectional connection (2.2-mV and 820- $\mu\text{V}$  EPSPs), and this was associated with putative synaptic contacts between an axon collateral and soma of one cell and a proximal dendrite and soma of the second cell (Fig. 2B).

Electrical synapses were also found among ELP neuron pairs. In only one case ( $<1\%$ ) did we find strong (i.e., high conductance) electrical coupling (Fig. 4, A and B); this was

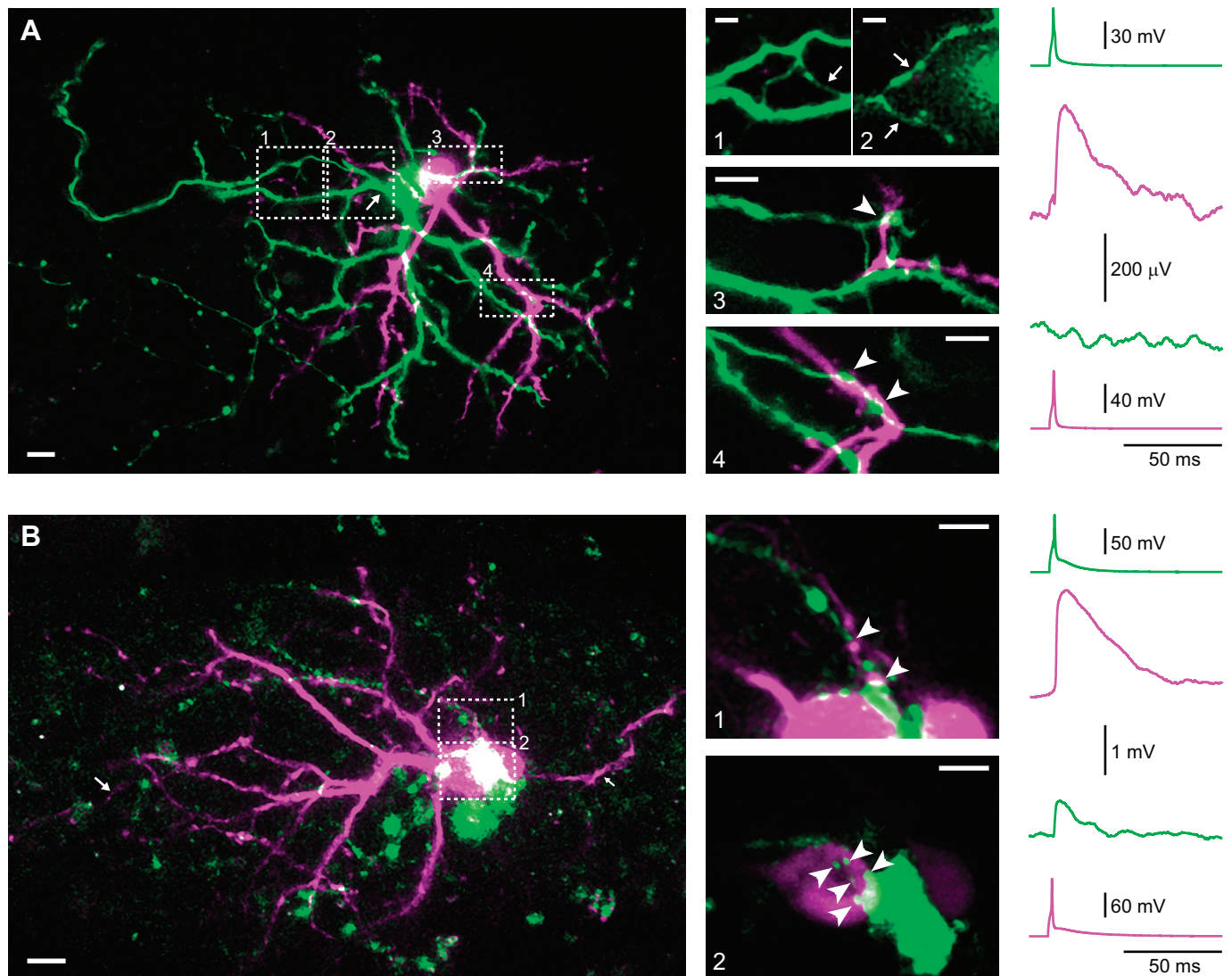


Fig. 2. Excitatory synaptic connections between ELP neurons. *A*: confocal images of a synaptically connected neuron pair filled with Alexa Fluor 488 (green) and 568 (magenta). Before imaging, each neuron was stimulated with brief current pulses to elicit time-locked spiking while recording the membrane potential of the other neuron, and the resulting voltage traces were averaged across 15 stimulus repetitions (traces on right). In this case, stimulation of the green neuron resulted in an excitatory postsynaptic potential (EPSP) in the magenta neuron (top 2 traces), but there was no evidence that the magenta neuron provided input to the green neuron (bottom 2 traces). In the view on left (scale bar, 10  $\mu\text{m}$ ), the broad dendritic arbors of both neurons are clearly visible, and the axon of the presynaptic green neuron can be seen emerging from the soma (arrow) and then forming numerous bifurcations. Expanded views of the areas enclosed by the 4 numbered boxes are shown at center (scale bars, 5  $\mu\text{m}$ ). In images 1 and 2, bifurcations of the axon that give rise to small collaterals are shown. A small collateral in image 1 (arrow) gives rise to a bifurcation visible in image 2. These 2 collaterals give rise to the axons visible in images 3 and 4 (upper arrow corresponds to branch leading to image 3, lower arrow corresponds to branch leading to image 4), where apparent boutons terminating onto dendrites of the magenta cell are visible (arrowheads). The images are based on maximum intensity projections of twenty-one 7.91- $\mu\text{m}$ -thick sections (left), four 2.86- $\mu\text{m}$ -thick sections (image 1), three 2.86- $\mu\text{m}$ -thick sections (image 2), seven 1.28- $\mu\text{m}$ -thick sections (image 3), and twelve 1.28- $\mu\text{m}$ -thick sections (image 4). *B*: in a second recorded pair, relatively large EPSPs occur in both directions. In this case, the green neuron had begun degrading before finishing imaging, so it was not possible to completely characterize its morphology or determine whether remaining neurites were axons or dendrites. Nevertheless, remnants of its cell body and proximal dendrites are visible in the view on left (scale bar, 10  $\mu\text{m}$ ), and potential synaptic contacts between the soma and an axon collateral of the magenta neuron with the soma and proximal dendrites of the green neuron are visible in the expanded, numbered views at center (arrowheads; scale bars, 5  $\mu\text{m}$ ). Also visible is a second magenta neuron just to the right of the green neuron, likely labeled as a result of electrical coupling with the recorded magenta neuron, as the same axon collateral shown in image 1 could be traced to the soma of the second labeled magenta neuron. The images are based on maximum intensity projections of twenty-five 7.00- $\mu\text{m}$ -thick sections (left) and three 1.28- $\mu\text{m}$ -thick sections (images 1 and 2).

between two low-pass neurons that were located directly next to each other ( $<5\text{-}\mu\text{m}$  distance). However, low-conductance electrical synapses were relatively common (63 of 407 pairs = 15.5%). These were evident as small spikelike potentials, or spikelets, coincident with presynaptic spikes and consisting of inward currents followed by outward currents (Fig. 4, *C* and *D*). Like the strongly coupled cells, these low-conductance couplings were bidirectional, although spikelet amplitude

could differ between the two cells. The amplitudes of these spikelets were generally quite small ( $70 \pm 30 \mu\text{V}$ ), although one was as large as 1.6 mV.

We also found “mixed” synapses, i.e., low-conductance electrical synapses co-occurring with excitatory synapses (Fig. 4, *E* and *F*). These were found in 16 cases, representing 25.0% of all pairs connected by electrical synapses and 25.8% of all pairs connected by excitatory synapses, or 3.9% of all neuron

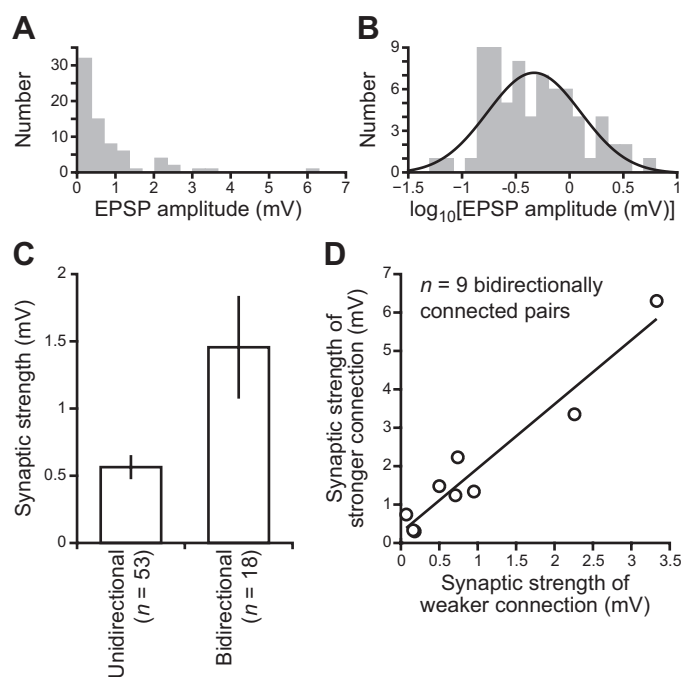


Fig. 3. Distribution of excitatory synaptic connection strengths is heavily skewed, and bidirectional connections are stronger than unidirectional connections. *A*: histogram of EPSP amplitudes resulting from spiking in a single presynaptic neuron reveals a distribution that is heavily skewed toward small values with a long tail at large values [Lilliefors test:  $KS(71) = 0.23$ ,  $P < 0.001$ ]. *B*: histogram of  $\log_{10}$ -transformed EPSP amplitudes reveals that synaptic strengths followed a log-normal distribution. Black line shows the best-fit normal distribution. [ $KS(71) = 0.08$ ,  $P > 0.3$ ]. *C*: bidirectional excitatory synaptic connections were characterized by significantly stronger synaptic strengths than unidirectional connections [Mann-Whitney  $U$ -test:  $z(53,18) = 2.63$ ,  $P < 0.01$ ]. *D*: the synaptic strengths of bidirectionally connected pairs were highly correlated, as seen in a plot of the stronger synaptic connection strength within a pair against the weaker synaptic connection strength within the pair (Spearman rank  $R = 0.85$ ;  $P < 0.01$ ).

pairs. Three of the neuron pairs with mixed synapses had bidirectional excitatory synapses (18.8%), whereas the remaining 13 had unidirectional excitatory synapses (81.2%). Intracellular fills of ELP neurons with biocytin during *in vivo* whole cell recording revealed both strong and weak dye coupling in several cases (Fig. 4*G*; see also Fig. 2*B*), providing further support for extensive gap junctional coupling among ELP neurons.

We found only two inhibitory synaptic connections (<1%), despite a concerted effort to record from somas of all sizes and locations along the surface of ELP, and to identify small outward currents by voltage-clamping cells at depolarized holding potentials (not shown). This is somewhat surprising given the hyperpolarizing synaptic potentials observed *in vivo* and *in vitro* (Carlson 2009; George et al. 2011), large numbers of GABAergic neurons throughout ELP (George et al. 2011), and strong effects of blocking GABA<sub>A</sub> receptors on the synaptic responses of ELP neurons (George et al. 2011). It is possible that inhibitory interactions occur along a superficial-deep axis, such that superficial neurons inhibit deep neurons and vice versa. We would have missed such connections because we were only able to visualize and record from neurons within  $\sim 20$ – $50$   $\mu\text{m}$  of the surface. Another possibility is that GABA release may be influenced by glutamate receptors on presynaptic terminals (Duguid and Smart 2004; Liu and

Lachamp 2006; Mathew and Hablitz 2011). If this is true, spiking of the inhibitory neuron itself may be insufficient to trigger inhibition in the absence of presynaptic excitation from a second neuron. Finally, individual inhibitory inputs may simply be too weak to detect, even at depolarized holding potentials. Future studies will test these hypotheses, but because of the lack of recordings from inhibitory connected neurons we focused on excitatory and electrical synaptic connections in this study.

*Excitatory connection probability and strength is greatest between neurons with similar IPI tuning.* A major advantage of our *in vitro* whole brain preparation is the ability to relate synaptic interactions between neurons to the function of those neurons in sensory coding. To determine how synaptic connectivity relates to IPI tuning, we analyzed the probability of excitatory synaptic connections, as well as synaptic strength and latency, as a function of the IPI tuning of recorded neuron pairs. Excitatory synapses were most common between neurons with similar tuning, e.g., high-pass/high-pass and low-pass/low-pass (Fig. 5*A*). High-pass neurons were significantly more likely to provide excitatory input to other high-pass neurons (26 of 107 pairs = 24.3%) than to neurons in the other tuning classes (11 of 120 pairs = 9.2%) [ $t(225) = 3.08$ ,  $P < 0.01$ ]. Similarly, low-pass neurons were significantly more likely to provide excitatory input to other low-pass neurons (9 of 47 pairs = 19.1%) than to neurons in the other tuning classes (4 of 85 pairs = 4.7%) [ $t(130) = 2.67$ ,  $P < 0.01$ ]. Band-pass neurons generally had a lower probability of providing excitatory input to other neurons, but they too were more likely to provide excitatory input to other band-pass neurons (2 of 24 pairs = 8.3%) than to neurons in the other tuning classes (2 of 82 pairs = 2.4%), although this difference was not significant [ $t(104) = 1.33$ ,  $P > 0.15$ ]. Because band-stop neurons were relatively rare, we did not obtain any simultaneous recordings from pairs of band-stop neurons, so we could not formally compare their connection probabilities with respect to IPI tuning. Bidirectional excitatory connections were more likely between neurons with similar tuning (7 of 195 pairs = 3.6%) than with different tuning (2 of 212 pairs = 0.9%), although the difference was not quite significant [ $t(405) = 1.81$ ,  $P = 0.07$ ].

Synaptic strength, as measured by EPSP amplitude, was significantly larger for connected pairs of neurons with similar IPI tuning compared with connected pairs with different IPI tuning (Fig. 5*B*) [Mann-Whitney  $U$ -test:  $z(41,30) = 2.72$ ,  $P < 0.01$ ]. The peak-to-peak and onset latencies of EPSPs did not, however, differ between similarly and differently tuned neurons (Fig. 5*B*) [ $z(41,30) = 0.42$ ,  $P > 0.6$ ;  $z(41,30) = 1.11$ ,  $P > 0.2$ ].

We also analyzed the probability of electrical synaptic connections as a function of the IPI tuning of recorded neuron pairs. Electrical synapses were generally less selective in their pattern of connectivity (Fig. 5*A*). High-pass neurons were more likely to have an electrical synaptic connection with other high-pass neurons (23 of 107 pairs = 21.5%) than with neurons in the other tuning classes (17 of 120 pairs = 14.2%), but this difference was not significant [ $t(224) = 1.48$ ,  $P > 0.1$ ]. Low-pass neurons were about equally likely to have an electrical synaptic connection with other low-pass neurons (6 of 47 pairs = 12.8%) as with neurons in the other tuning classes (12 of 85 pairs = 14.1%) [ $t(130) = 0.22$ ,  $P > 0.8$ ]. Band-pass

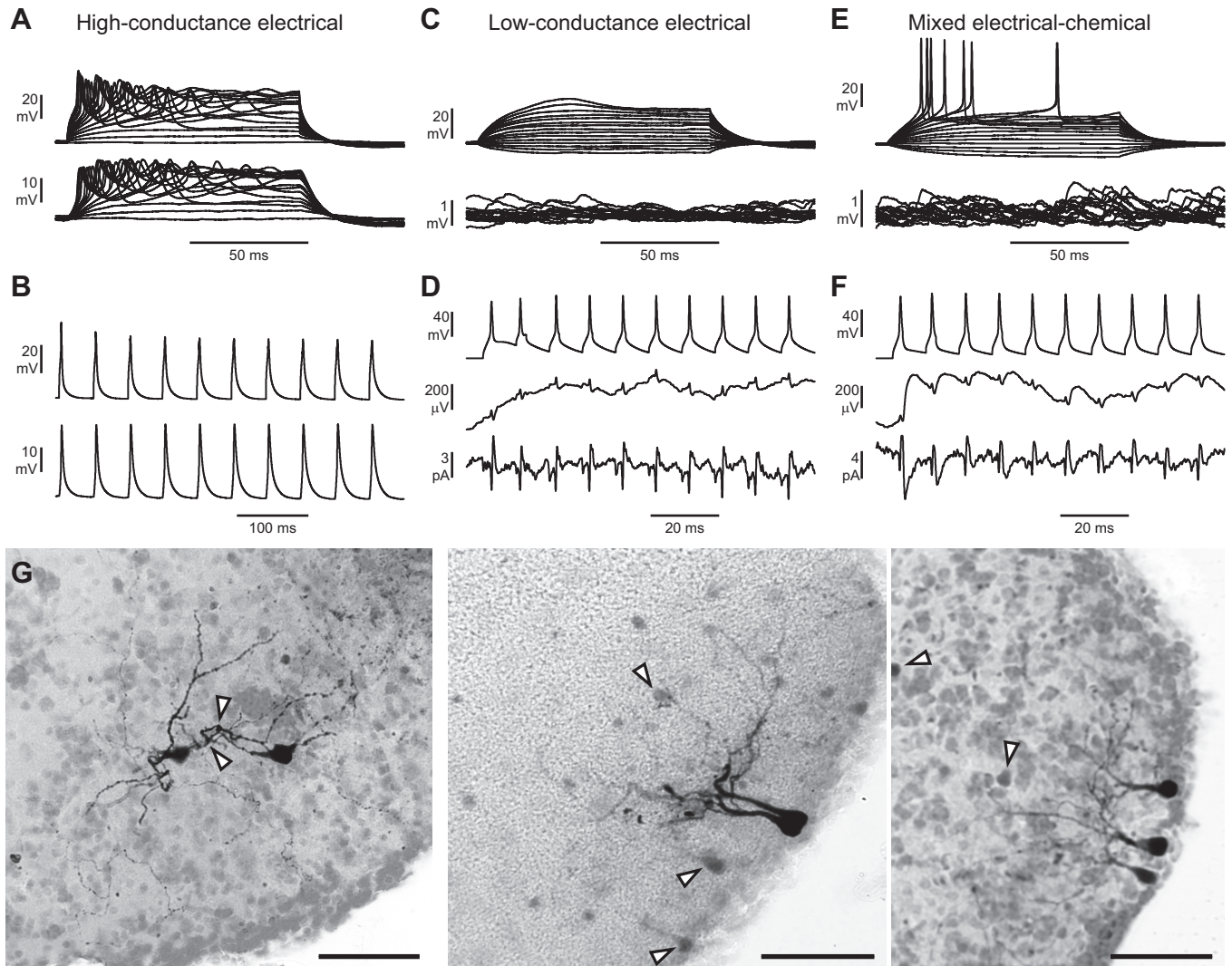


Fig. 4. Electrical coupling between ELP neurons. *A*: a high-conductance electrical synapse between 2 ELP neurons. Current steps applied to neuron shown in *top* trace led to clear voltage changes in both neurons; when these steps were above threshold, both neurons fired action potentials. *B*: responses of the same 2 neurons to trains of short depolarizing current pulses applied only to neuron in *top* trace (50-ms IPI). Both cells spiked in response to each stimulus pulse. *C*: example of a low-conductance electrical synapse between 2 ELP neurons. Current steps applied to neuron shown in *top* trace did not cause clear voltage changes in neuron shown in *bottom* trace. *D*: responses of same 2 neurons to trains of short depolarizing current pulses applied only to neuron in *top* trace (10-ms IPI). The stimulated neuron spikes in response to each stimulus pulse (*top*), and small spikelets in the second cell that are coincident with these spikes can be seen under current clamp (*middle*) and inward/outward currents can be seen under voltage clamp (*bottom*). *E*: example of a mixed chemical-electrical synaptic connection between 2 ELP neurons. Current steps applied to neuron shown in *top* trace did not cause clear voltage changes in neuron shown in *bottom* trace. *F*: responses of same 2 neurons to trains of short depolarizing current pulses applied only to neuron in *top* trace (10-ms IPI). The stimulated neuron spikes in response to each stimulus pulse (*top*). In the second cell, small spikelets that are coincident with these spikes can be seen under current clamp, and these are followed by slower depolarizing potentials (*middle*). Inward/outward currents that are coincident with these spikes can be seen under voltage clamp, and these are followed by slower inward currents (*bottom*). *G*: examples of dye coupling among ELP neurons (scale bars, 50 μm). Individual cells were filled with biocytin during *in vivo* recordings. After processing the tissue, multiple stained cells were often visible. *Left*: strong dye coupling between 2 neurons, along with apparent points of synaptic contact (arrowheads). *Center*: strong dye coupling between 2 neurons located directly adjacent to each other, along with weak dye coupling with several neurons (e.g., arrowheads). *Right*: strong dye coupling between 3 neurons, along with weak dye coupling with several neurons (e.g., arrowheads).

neurons were also about equally likely to have an electrical synaptic connection with other band-pass neurons (4 of 24 pairs = 16.7%) as with neurons in the other tuning classes (15 of 82 pairs = 18.3%) [ $t(104) = 0.18$ ,  $P > 0.8$ ].

**Excitatory and electrical connection probabilities decrease with distance.** In cortical microcircuits, excitatory connection probabilities decrease with distance (Perin et al. 2011). To determine how synaptic connectivity relates to the distance between neurons, we analyzed the probability of excitatory synaptic connections, as well as synaptic strength and latency, as a function of the intersomatic distance between recorded

neuron pairs. Excitatory synapses were most common when the distance between recorded somas was relatively small (Fig. 5C). No excitatory synaptic connections were detected at distances  $> 54 \mu\text{m}$ , despite recording from 53 pairs of neurons at distances ranging from 50 to 381 μm. Thus there was a strong negative correlation between distance and probability of excitatory synaptic connection (Spearman rank  $R = -0.86$ ;  $P < 0.0001$ ). However, the distance between pre- and post-synaptic somas did not correlate with synaptic strength (EPSP amplitude) (Spearman rank  $R = -0.04$ ;  $P > 0.7$ ), peak-to-peak latency (Spearman rank  $R = 0.07$ ;  $P > 0.5$ ), or onset

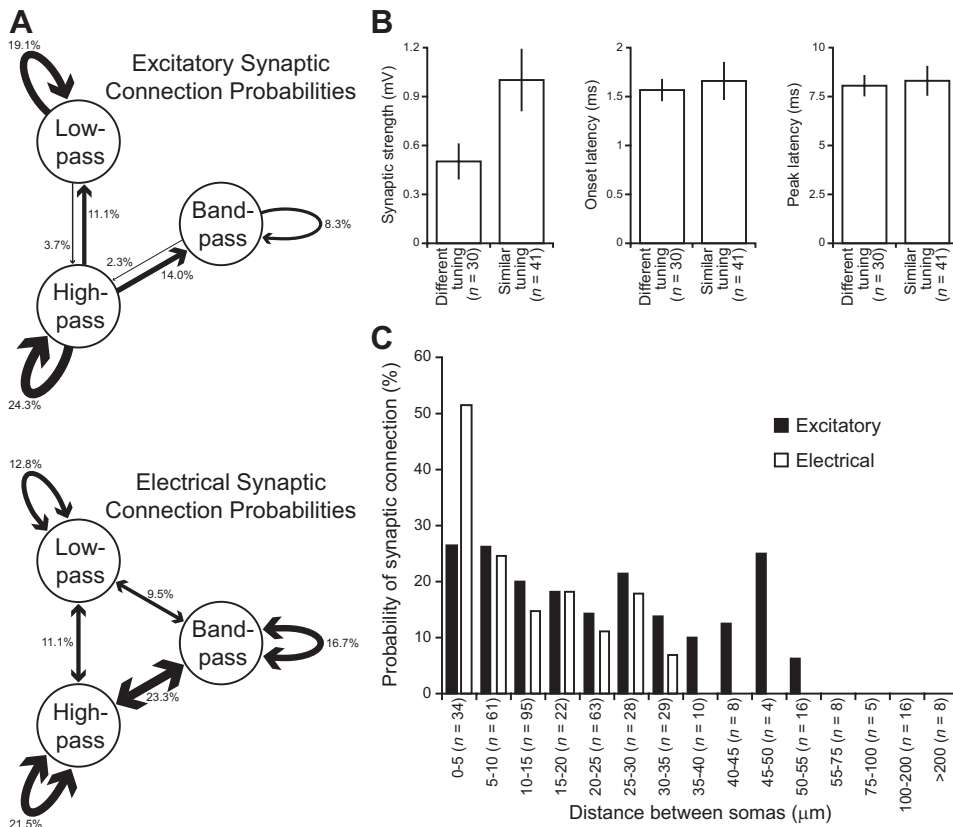


Fig. 5. Synaptic connection probability varies with IPI tuning and distance, and synaptic strength varies with IPI tuning. *A*: connection diagrams illustrating excitatory synaptic connection probabilities (*top*) and electrical synaptic connection probabilities (*bottom*) among low-, band-, and high-pass neurons. Arrows indicate directionality of the connections, and line thickness indicates relative differences in connection probabilities, with text labels indicating the actual probability of a synaptic connection. All electrical synaptic connections were bidirectional. *B*: for excitatory synaptic connections, synaptic strength (EPSP amplitude) was significantly larger for connected neurons with similar IPI tuning than connected neurons with different IPI tuning [Mann-Whitney *U*-test:  $z(41,30) = 2.72, P < 0.01$ ]. There was no significant difference in latencies to EPSP onset [ $z(41,30) = 1.11, P > 0.2$ ] or peak [ $z(41,30) = 0.42, P > 0.6$ ]. *C*: probability of excitatory and electrical synaptic connections with respect to distance between recorded somas. Sample sizes show the numbers of neuron pairs recorded at each range of distances.

latency (Spearman rank  $R = 0.03; P > 0.7$ ). Electrical synapses were even more limited in their spatial extent, with none detected at distances  $> 30 \mu\text{m}$ . Thus there was also a strong negative correlation between distance and probability of electrical synaptic connection (Spearman rank  $R = -0.90; P < 0.00001$ ).

*Rate-dependent depression is ubiquitous at excitatory synapses between neurons.* Short-term synaptic plasticity and temporal summation have both been identified as mechanisms for temporal filtering at synapses (Fortune and Rose 2001; George et al. 2011). To characterize short-term plasticity and temporal summation at the excitatory synapses between ELP neurons, we examined synaptic responses to presynaptic spike trains of 10 pulses with IPIs of 10, 50, or 100 ms (e.g., Fig. 6A). We did not observe synaptic facilitation in any of these recordings; instead we observed clear synaptic depression of both EPSPs and EPSCs at

every excitatory synapse tested at all three IPIs (Fig. 6). Analyzing the change in normalized peak synaptic current as a function of pulse number under voltage clamp revealed a significant decrease in synaptic currents [repeated-measures ANOVA:  $F(8,136) = 14.89, P < 0.000001$ ]. There was also a significant interaction effect between IPI and pulse number [ $F(16,272) = 5.17, P < 0.000001$ ], reflecting a greater decrease in synaptic current during the 10- and 50-ms IPI trains compared with the 100-ms IPI train (Fig. 6B). At the shortest IPI tested (10 ms), temporal summation counteracted the effects of depression (Fig. 6A), causing the total synaptic current in response to the second pulse to remain relatively high, and leading to a similar overall decrease in synaptic current compared with 50-ms IPIs (Fig. 6B).

To test whether synaptic depression at the excitatory synapses between ELP neurons varies with respect to IPI tuning, we performed additional statistical tests. First, we

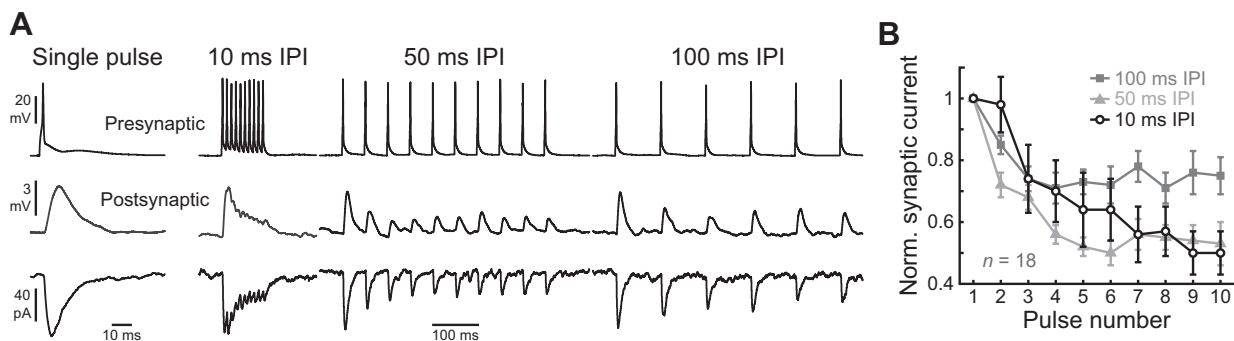


Fig. 6. Excitatory synaptic connections among ELP neurons are characterized by rate-dependent depression. *A*: synaptic potentials and synaptic currents in response to stimulating neuron in *top* trace with short depolarizing current pulses delivered singly or in 10-ms, 50-ms, or 100-ms IPI trains, after averaging across 15 repetitions. *B*: change in normalized synaptic current as a function of pulse number and IPI among 18 postsynaptic neurons.

added an independent variable to our repeated-measures ANOVA to compare the amount of depression at synapses between similarly tuned neurons (e.g., high-pass and high-pass,  $n = 10$ ) to the amount of depression at differently tuned neurons (e.g., high-pass and low-pass,  $n = 8$ ). However, there was no significant interaction effect between pulse number and similar versus different tuning [ $F(8,128) = 1.19$ ,  $P > 0.3$ ] or between pulse number, IPI, and similar versus different tuning [ $F(16,256) = 0.73$ ,  $P > 0.7$ ]. Then we performed two similar analyses, first comparing presynaptic high-pass ( $n = 10$ ) versus low-pass ( $n = 3$ ) neurons and then comparing postsynaptic high-pass ( $n = 8$ ) versus low-pass ( $n = 5$ ) neurons. Again, there was no significant interaction effect between pulse number and tuning type [presynaptic:  $F(8,88) = 1.42$ ,  $P > 0.1$ ; postsynaptic:  $F(8,88) = 0.43$ ,  $P > 0.8$ ] or between pulse number, IPI, and tuning type [presynaptic:  $F(16,176) = 0.90$ ,  $P > 0.5$ ; postsynaptic:  $F(16,176) = 1.45$ ,  $P > 0.1$ ]. Thus rate-dependent depression appears to be ubiquitous at excitatory synapses between ELP neurons, and there is no evidence that its kinetics are adapted to the IPI tuning of pre- or postsynaptic neurons.

*Excitatory synaptic transmission involves both NMDA and non-NMDA glutamate receptors.* Fast glutamatergic synaptic transmission is typically mediated by non-NMDA receptors, whereas synaptic potentials mediated by NMDA receptors generally have a slower onset and a longer duration as well as voltage dependence (Andreasen et al. 1988, 1989; Forsythe and Westbrook 1988; McBain and Mayer 1994). To determine whether both types of receptors contribute to excitatory synaptic transmission in ELP, we bath applied the NMDA receptor antagonist APV and the non-NMDA receptor antagonist DNQX. Application of either drug reduced depolarizing synaptic responses (EPSPs) to ELA stimulation (e.g., Fig. 7A). Blocking NMDA receptors with APV led to a significant reduction in EPSP amplitude [Wilcoxon matched-pairs test:  $z(47) = 4.62$ ,  $P < 0.00001$ ] as well as a significant decrease in latency to the peak [ $z(47) = 4.15$ ,  $P < 0.0001$ ], suggesting a selective effect on slow EPSP components (Fig. 7B). Blocking non-NMDA receptors with DNQX also led to a significant reduction in EPSP amplitude [ $z(56) = 6.25$ ,  $P < 0.000001$ ] but a significant increase in latency to the peak [ $z(56) = 5.16$ ,  $P < 0.000001$ ], suggesting a selective effect on fast EPSP components (Fig. 7B). Blocking both receptors eliminated synaptic

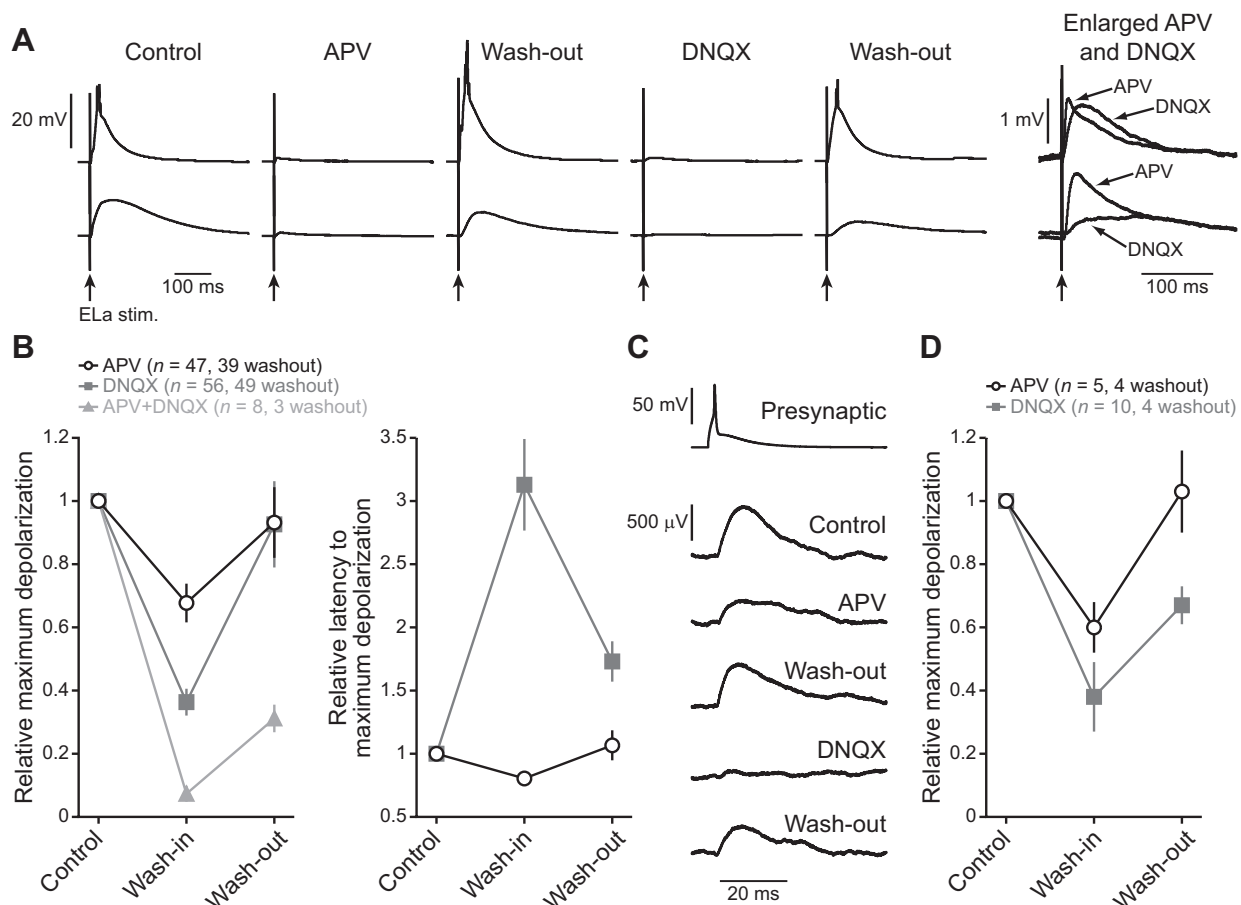


Fig. 7. Excitatory synaptic transmission relies on both slow NMDA and fast non-NMDA glutamate receptors. *A*: average synaptic potentials of 2 simultaneously recorded ELP neurons in response to ELA stimulation before, during, and after application of the NMDA receptor antagonist DL-2-amino-5-phosphonopentanoic acid (APV) and the non-NMDA receptor antagonist 6,7-dinitroquinoxaline-2,3-dione (DNQX). *B*: effects of APV and DNQX on maximum synaptic depolarization and latency to maximum synaptic depolarization in response to ELA stimulation, normalized to predrug control values (means  $\pm$  SE). *C*: average synaptic potentials of a single ELP neuron in response to stimulation of a presynaptic ELP neuron before, during, and after application of the NMDA receptor antagonist APV and the non-NMDA receptor antagonist DNQX. *D*: effects of APV and DNQX on maximum synaptic depolarization in response to stimulation of a single presynaptic neuron, normalized to predrug control values (means  $\pm$  SE).

responses to within recording noise levels [ $z(8) = 2.52, P < 0.05$ ] (Fig. 7B). For the cells that we were able to test with both drugs, DNQX caused a significantly larger decrease in synaptic response compared with APV [ $z(40) = 3.34, P < 0.001$ ].

In other sensory circuits, slow NMDA receptors and fast non-NMDA receptors have been shown to play distinct roles in temporal filtering (Daw et al. 1993). However, the effects of APV and DNQX on single-pulse responses did not differ with respect to IPI tuning [APV:  $F(5,41) = 1.58, P > 0.1$ ; DNQX:  $F(5,50) = 1.17, P > 0.3$ ]. Interestingly, application of either drug resulted in a shift toward high-pass tuning. Of 24 neurons, application of DNQX caused the number of high-pass neurons to increase from 10 (41.7%) to 19 (79.2%) [ $t(46) = 2.66, P < 0.05$ ] and the number of low-pass neurons to decrease from 4 (16.7%) to 0 (0.0%) [ $t(46) = 2.09, P < 0.05$ ]. Of 32 neurons, application of APV caused the number of high-pass neurons to increase from 9 (28.1%) to 18 (56.2%) [ $t(62) = 2.28, P < 0.05$ ] and the number of low-pass neurons to decrease from 9 (28.1%) to 4 (12.5%) [ $t(62) = 1.55, P > 0.1$ ]. Thus the interplay between both receptor types may be important in establishing variation in temporal filtering among ELP neurons.

To directly examine whether NMDA and non-NMDA receptors contribute to excitation between ELP neurons, we bath applied APV and DNQX during paired recordings from neurons having excitatory synaptic connections (e.g., Fig. 7C). In every pair tested, application of APV led to a decrease in EPSP amplitude [ $z(5) = 2.02, P < 0.05$ ] and application of DNQX also led to a decrease in EPSP amplitude [ $z(10) = 2.70, P < 0.01$ ] (Fig. 7D). The synaptic responses under these conditions were too small to reliably measure synaptic latencies. In five connected neuron pairs, we were able to test DNQX and APV separately, and in every case both drugs reduced EPSP amplitudes (e.g., Fig. 7C). Thus individual excitatory synaptic connections between ELP neurons appear to be mediated by both NMDA and non-NMDA glutamate receptors.

*Direct and indirect synaptic connections contribute to temporal selectivity.* To investigate the contribution of individual neurons to the IPI tuning of other neurons in the circuit, we silenced neurons that normally spiked in response to ELA stimulation by hyperpolarizing the membrane potential to  $\sim -90$  mV. First, we determined the IPI tuning of both neurons under control conditions. Then, we silenced the spiking neuron and determined the IPI tuning of the other neuron. Synaptic responses were affected in every pair of neurons having an excitatory (e.g., Fig. 8A) or electrical (e.g., Fig. 8B) synaptic

connection. In neuron pairs having an excitatory synaptic connection, three of five (60%) postsynaptic neurons changed their tuning categorization after silencing the presynaptic cell. Similarly, three of four (75%) neurons having an electrical synaptic connection changed their tuning categorization after silencing the spiking cell.

Given the high connectivity of this circuit, it is unlikely that the observed changes in response were due solely to the direct connection between the two cells. To determine the degree to which indirect synaptic connections could affect responses, we silenced spiking cells while determining the IPI tuning of a second neuron that did not have any apparent synaptic connection with the spiking neuron. In several cases, this also had a strong effect on synaptic responses to ELA stimulation (Fig. 8C). Twelve of twenty-two (54.5%) nonconnected neurons changed their tuning categorization after the spiking neuron was silenced, indicating indirect effects mediated by interneurons and further suggesting dense connectivity among ELP neurons that contributes to IPI tuning.

To quantify the effects of silencing neurons on the responses of other neurons, we measured the absolute values of the differences in maximum synaptic potentials before and during silencing across all IPI stimuli and then averaged across stimuli. Neurons receiving a chemical excitatory input from the spiking cell were affected the most, followed by neurons with an electrical synaptic connection, and finally neurons with no apparent synaptic connection (Fig. 8D) [ANOVA:  $F(2,28) = 4.33, P < 0.01$ ].

## DISCUSSION

We found high levels of excitatory connectivity, consistent with the extensive dendritic arbors and intrinsic axonal projections of ELP neurons (George et al. 2011; Xu-Friedman and Hopkins 1999). Excitatory connection probabilities were greatest among similarly tuned neurons located within  $50 \mu\text{m}$  of each other, and excitatory connection strengths were greatest among similarly tuned neurons (Fig. 9A). These excitatory interactions were mediated by both NMDA and non-NMDA glutamatergic signaling, and they contributed to the temporal selectivity of individual neurons.

We hypothesize that the relatively large number of strong inputs from similarly tuned neurons reinforce the general IPI tuning pattern (e.g., high-pass vs. low-pass) and contribute to variation in tuning curve shape, whereas the relatively small number of weak inputs from differently tuned neurons alter IPI

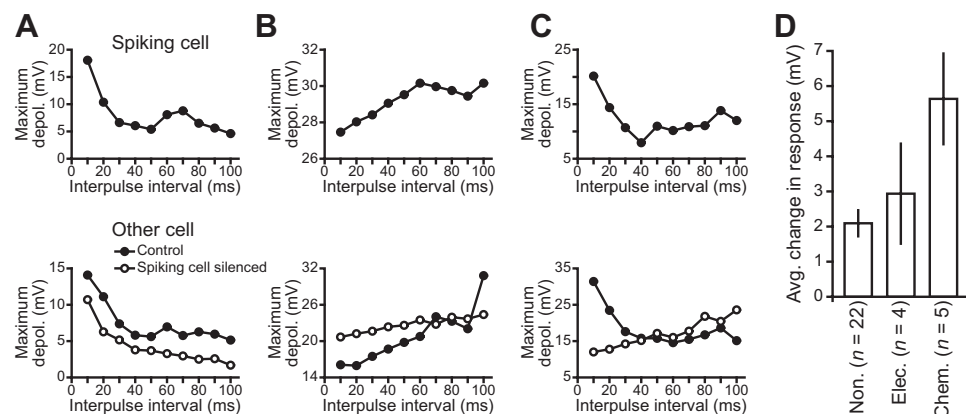


Fig. 8. Single neurons contribute to the IPI tuning of other neurons. A–C: examples of changes in response when a spiking cell that provided excitatory synaptic input (A), electrical synaptic input (B), or no direct synaptic input (C) to the other recorded cell was silenced by hyperpolarization. The IPI tuning of the spiking cell is shown at top, and the IPI tuning of the other cell, before and during silencing of the spiking cell, is shown at bottom. D: average change in response across all IPIs was largest for excitatory synaptic connections (Chem) and smallest for nonconnected neurons (Non).

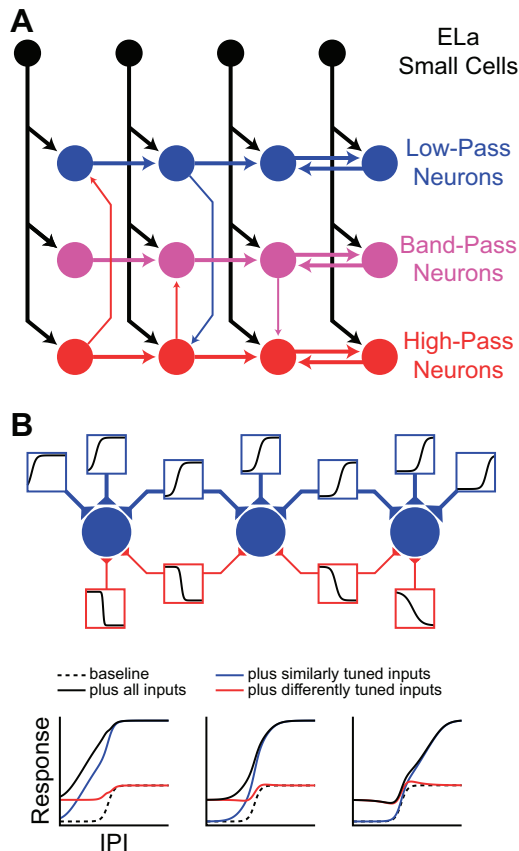


Fig. 9. Schematics summarizing local excitatory network connectivity in ELP and the hypothesized role for network interactions in shaping IPI tuning. **A:** schematic summarizing the excitatory network topology of ELP. Small cells from ELA project topographically to ELP, synapsing onto ELP neurons throughout its anterior-posterior extent (Friedman and Hopkins 1998). Individual ELP neurons are more likely to provide excitatory input to nearby neurons (Fig. 5C), they are more likely to provide excitatory input to similarly tuned neurons (Fig. 5A), and their excitatory connections with similarly tuned neurons are stronger than their excitatory connections with differently tuned neurons (Fig. 5B). **B:** hypothesized role of local excitatory interactions in shaping IPI tuning. Three low-pass neurons are shown, and they all have the same IPI tuning in the absence of local excitatory inputs. This baseline IPI tuning could arise because of local inhibitory input or short-term depression of excitatory input from ELA (Baker et al. 2013; George et al. 2011). Each neuron receives strong excitatory input from 3 low-pass neurons and weak excitatory input from 2 high-pass neurons, each with a different tuning curve. Relative to baseline tuning, the strong excitatory inputs are scaled to 0.6 and the weak excitatory inputs are scaled to 0.3 to simulate the effects of these inputs on IPI tuning. The strong excitatory inputs from similarly tuned neurons reinforce the low-pass tuning of each neuron but also contribute to variation in the shape of their tuning curves. The weak excitatory inputs from differently tuned neurons contribute to variation in tuning curve shape without changing the basic pattern of tuning. Each neuron has a distinct tuning curve because they each receive a unique combination of local excitatory inputs.

tuning in more subtle ways (Fig. 9B). The shapes of IPI tuning curves vary among the population of ELP neurons, both in vivo (Carlson 2009) and in vitro (George et al. 2011). Because of this diversity, changes in IPI will be represented by changes in the population of responsive ELP neurons, thereby converting a temporal code into a population code (Baker et al. 2013). We suggest that IPI tuning diversity is established, in part, by each individual neuron receiving a unique complement of local excitatory inputs (Fig. 9B). Population codes are common in central sensory pathways, as they are an efficient means of accurately representing a large number of stimuli (Averbeck et

al. 2006). By contributing to variation in stimulus tuning among neurons, the types of network interactions we describe here may prove to be a fundamental mechanism for increasing the precision of population coding.

**Excitatory interactions in sensory microcircuits.** Multineuron intracellular recordings, photostimulation, and optical imaging have been performed extensively in slice preparations of rodent sensory cortex to elucidate cortical microcircuitry. We found a number of similarities between cortical and ELP connectivity patterns. Synapses in both circuits are characterized by short-term depression (De Pasquale and Sherman 2011; Perin et al. 2011; Reig et al. 2006; Reyes et al. 1998). The probability of a chemical excitatory connection between adjacent cortical pyramidal neurons is similar to ELP, ~10–20% (Markram et al. 1997; Yoshimura et al. 2005), and these connection probabilities also decrease with distance (Perin et al. 2011). In addition, bidirectional synaptic connections in ELP were significantly stronger than unidirectional connections and bidirectional connection strengths were correlated, both of which are also features of cortical microcircuitry (Song et al. 2005).

Cortical pyramidal neurons tend to cluster into highly connected assemblies of a few dozen neurons each (Perin et al. 2011; Song et al. 2005; Yoshimura et al. 2005). The exact functional significance of these assemblies remains unknown, but mounting evidence suggests they play an important role in information processing and sensory perception: stimulation of single cortical neurons can have wide-ranging effects on cortical activity in vivo (Kwan and Dan 2012), and this can influence sensory perception (Houweling and Brecht 2008), evoke movements (Brecht et al. 2004), and modify global brain state (Li et al. 2009). Furthermore, neurons in visual cortex that have the same orientation tuning are significantly more likely to share a connection than neurons with orthogonal orientation tuning (Ko et al. 2011). Although we cannot yet determine whether similar assemblies exist within ELP, our results suggest this is likely.

Variation in synaptic strength in both ELP and cortex conforms to a log-normal distribution, in which weak synapses are common and strong synapses are rare (Song et al. 2005). A log-normal distribution of synaptic connection strengths may be a natural consequence of the activity-dependent rules governing long-term synaptic plasticity (Song et al. 2005). Indeed, the existence of NMDA receptors at the synapses between ELP neurons raises the intriguing possibility of spike timing-dependent plasticity in the circuit (Bell et al. 1997b; Dan and Poo 2004; Shouval et al. 2002). It will be interesting to determine whether long-term plasticity occurs in ELP and, if so, its time course and behavioral relevance to the processing of electric communication signals. Although our understanding of ELP microcircuitry clearly lags far behind our understanding of cortical microcircuitry, the mormyrid system has the advantage that it is more straightforward to draw links between neuronal activity in vitro and its relevance to behavior and sensory processing in vivo (Baker et al. 2013).

**Electrical coupling in sensory microcircuits.** We also found extensive electrical coupling among ELP neurons, based on both paired recordings and dye coupling. Electrical connection probabilities decreased steeply with distance, from as high as 50% at distances of  $<5 \mu\text{m}$  to 0% beyond  $35 \mu\text{m}$ . The effects of these apparent gap junctions on voltages at the soma were

relatively small in all but one case. Although they may not strongly influence somatic voltage individually, their effects on local synaptic integration within dendritic arbors could still shape information processing by ELP neurons, as suggested by the effects of silencing electrically coupled neurons on IPI tuning. For example, weak electrical synapses could enhance or sharpen the temporal precision of coincidence detection in dendrites (Harnett et al. 2012; Takahashi et al. 2012) or shape responses to the temporal sequence in which different dendritic inputs are activated (Branco et al. 2010; Branco and Häusser 2011). Furthermore, it is likely that large numbers of electrical synapses from many neurons will be active in response to sensory stimuli, which together could drive spike synchrony or desynchrony across the network (Vervaeke et al. 2010; Wang et al. 2010) as well as shape longer-term modulations in firing rate (Vandecasteele et al. 2005).

*Multiple mechanisms for temporal processing.* Temporal sequences are important components of many sensory stimuli, especially communication signals (Pollack 2001). Neural mechanisms for the processing of temporal sequences have been studied in several different vertebrate sensory pathways (Baker et al. 2013; Rose 1986; Rose and Fortune 1999). A common theme has emerged, in which timing- or rate-dependent shifts in the balance between excitation and inhibition can arise from mechanisms such as short-term synaptic plasticity, temporal summation of synaptic inputs, and differences in the relative timing or durations of synaptic inputs (Edwards et al. 2007, 2008; Fortune and Rose 2001; George et al. 2011; Klug et al. 2012; Rose et al. 2011). Passive and active membrane properties can also contribute to temporal filtering (Carlson and Kawasaki 2006; Fortune and Rose 1997, 2003). However, out of practical necessity, these studies have largely focused on synaptic integration and cellular physiology in individual cells, and not on the underlying network architecture that establishes variation in synaptic inputs. In the present study, we reveal that local excitatory interactions can also influence the processing of temporal sequences.

Each excitatory synapse was characterized by rate-dependent short-term depression (Zucker and Regehr 2002). The attenuation of EPSPs at short IPIs would seem to establish low-pass tuning in the circuit (Baker et al. 2013). However, we do not yet know the nature of short-term plasticity at ELA-to-ELP synapses, or in the inhibitory pathways to ELP neurons, so the balance between depression of excitation and inhibition remains unknown. In addition, a large number of excitatory inputs are activated in response to sensory stimulation or stimulation of incoming ELA axons (Carlson 2009; George et al. 2011), resulting in spatial summation. The effects of temporal summation on these spatially summated EPSPs contribute substantially to IPI tuning (George et al. 2011). We suggest that short-term depression, temporal summation, and variation in the relative timing of synaptic inputs establish temporal filtering through synaptic integration within ELP neurons, and that network interactions among ELP neurons serve to enhance and diversify this temporal filtering (Fig. 9). Thus the IPI tuning of an individual neuron reflects both the IPI tuning of its inputs as well as the spatiotemporal integration of those inputs.

*The coding of multiple stimulus features.* In many sensory systems, lateral interactions between neurons are important in spatial analysis (Bell et al. 1997a; Hartline 1969; Khosravi-Hashemi et al. 2011; Sachdev et al. 2012). By directly stimu-

lating the afferent inputs to ELP, we effectively mimicked sensory stimulation of the entire body surface, allowing us to focus on the role of network interactions in temporal processing. However, these interactions may also be involved in the spatial analysis of electric signals. During natural communication behavior, the spatial extent of electrosensory stimulation on the receiving fish's body will vary as the relative location and orientation of the signaling fish change (Schluger and Hopkins 1987). In addition to their IPI tuning, ELP neurons recorded *in vivo* respond selectively to pulse duration and intensity as well as the location and orientation of signaling fish (Amagai 1998). The initial analysis of these other features appears to be performed in ELA (Friedman and Hopkins 1998). Small cells, the only ELA output neurons, project topographically to ELP (Friedman and Hopkins 1998). They traverse the border between ELA/ELP to the distal edge of ELP while maintaining their medio-lateral position, giving off en passant synaptic boutons onto dendrites throughout their length (Friedman and Hopkins 1998). The topographic input from small cells suggests there may be a spatial representation of electric signal features in ELP, but we do not yet know whether small cells actually represent stimulus information topographically. They receive excitatory input from elongated axons that follow a convoluted path through ELA (Friedman and Hopkins 1998), making it unlikely for there to be any precise mapping of temporal or spatial features (Xu-Friedman and Hopkins 1999). However, the inhibitory input to small cells is more direct (Friedman and Hopkins 1998), and this could contribute to a spatial representation of stimulus information in ELA.

*Toward a network model of temporal processing.* Our findings were facilitated by the development of an *in vitro* whole brain preparation in a model system that allows for simultaneous intracellular recording from multiple neurons, precisely timed synaptic stimulation, and pharmacological manipulation, all while keeping neuronal circuitry intact. Furthermore, the unique characteristics of this sensory pathway allow us to directly relate temporal patterns of synaptic stimulation to the processing of natural stimuli (Carlson 2009; George et al. 2011). This preparation will facilitate future technical directions including simultaneous recordings from more than two neurons, "blind" recordings from deep neurons combined with visualized recordings from superficial neurons, simultaneous recordings from neurons in ELA and ELP, calcium imaging of cell populations and dendritic integration, detailed anatomical studies of functional variation in synaptic morphology and location along dendritic arbors, and spatially precise neurotransmitter agonist and antagonist delivery. Combining these approaches will eventually allow us to construct a comprehensive model of electric signal processing that incorporates the morphology and synaptic and cellular physiology of individual neurons along with the network interactions among those neurons.

#### ACKNOWLEDGMENTS

Thanks to Dianne Duncan and Elizabeth Haswell for assistance with confocal imaging.

## GRANTS

This work was supported by a grant from the National Science Foundation (IOS-1050701 to B. A. Carlson) and a fellowship from the Japan Society for the Promotion of Science (G2205 to T. Kohashi).

## DISCLOSURES

No conflicts of interest, financial or otherwise, are declared by the author(s).

## AUTHOR CONTRIBUTIONS

Author contributions: X.M., T.K., and B.A.C. conception and design of research; X.M., T.K., and B.A.C. performed experiments; X.M. and B.A.C. analyzed data; X.M., T.K., and B.A.C. interpreted results of experiments; X.M., T.K., and B.A.C. edited and revised manuscript; X.M., T.K., and B.A.C. approved final version of manuscript; B.A.C. prepared figures; B.A.C. drafted manuscript.

## REFERENCES

- Ahrens MB, Keller PJ. Whole-brain functional imaging at cellular resolution using light-sheet microscopy. *Nat Methods* 10: 413–420, 2013.
- Amagai S. Time coding in the midbrain of mormyrid electric fish. II. Stimulus selectivity in the nucleus extero-lateralis pars posterior. *J Comp Physiol A* 182: 131–143, 1998.
- Andreasen M, Lambert JD, Jensen MS. Direct demonstration of an *N*-methyl-D-aspartate receptor mediated component of excitatory synaptic transmission in area CA1 of the rat hippocampus. *Neurosci Lett* 93: 61–66, 1988.
- Andreasen M, Lambert JD, Jensen MS. Effects of new non-*N*-methyl-D-aspartate antagonists on synaptic transmission in the in vitro rat hippocampus. *J Physiol* 414: 3147–3336, 1989.
- Arnegard ME, Carlson BA. Electric organ discharge patterns during group hunting by a mormyrid fish. *Proc Biol Sci* 272: 1305–1314, 2005.
- Averbeck BB, Latham PE, Pouget A. Neural correlations, population coding and computation. *Nat Rev Neurosci* 7: 358–366, 2006.
- Baker C, Kohashi T, Lyons-Warren A, Ma X, Carlson B. Multiplexed temporal coding of electric communication signals in mormyrid fishes. *J Exp Biol*. In press.
- Bell CC, Caputi A, Grant K. Physiology and plasticity of morphologically identified cells in the mormyrid electrosensory lobe. *J Neurosci* 17: 6409–6423, 1997a.
- Bell CC, Han VZ, Sugawara Y, Grant K. Synaptic plasticity in a cerebellum-like structure depends on temporal order. *Nature* 387: 278–281, 1997b.
- Branco T, Clark BA, Häusser M. Dendritic discrimination of temporal input sequences in cortical neurons. *Science* 329: 1671–1675, 2010.
- Branco T, Häusser M. Synaptic integration gradients in single cortical pyramidal cell dendrites. *Neuron* 69: 885–892, 2011.
- Brecht M, Schneider M, Sakmann B, Margrie TW. Whisker movements evoked by stimulation of single pyramidal cells in rat motor cortex. *Nature* 427: 704–710, 2004.
- Brown SP, Hestrin S. Intracortical circuits of pyramidal neurons reflect their long-range axonal targets. *Nature* 457: 1133–1136, 2009.
- Carlson BA. Electric signaling behavior and the mechanisms of electric organ discharge production in mormyrid fish. *J Physiol (Paris)* 96: 405–419, 2002a.
- Carlson BA. Neuroanatomy of the mormyrid electromotor control system. *J Comp Neurol* 454: 440–455, 2002b.
- Carlson BA. A neuroethology of electrocommunication: senders, receivers, and everything in between. In: *Communication in Fishes*, edited by Ladich F, Collin SP, Moller P, Kapoor BG. Enfield, NH: Science Publishers, 2006, p. 805–848.
- Carlson BA. Temporal-pattern recognition by single neurons in a sensory pathway devoted to social communication behavior. *J Neurosci* 29: 9417–9428, 2009.
- Carlson BA, Kawasaki M. Stimulus selectivity is enhanced by voltage-dependent conductances in combination-sensitive neurons. *J Neurophysiol* 96: 3362–3377, 2006.
- Dan Y, Poo MM. Spike timing-dependent plasticity of neural circuits. *Neuron* 44: 23–30, 2004.
- Daw N, Stein P, Fox K. The role of NMDA receptors in information processing. *Annu Rev Neurosci* 16: 207–222, 1993.
- De Pasquale R, Sherman SM. Synaptic properties of corticocortical connections between the primary and secondary visual cortical areas in the mouse. *J Neurosci* 31: 16494–16506, 2011.
- Duguid IC, Smart TG. Retrograde activation of presynaptic NMDA receptors enhances GABA release at cerebellar interneuron-Purkinje cell synapses. *Nat Neurosci* 7: 525–533, 2004.
- Edwards CJ, Leary CJ, Rose GJ. Counting on inhibition and rate-dependent excitation in the auditory system. *J Neurosci* 27: 13384–13392, 2007.
- Edwards CJ, Leary CJ, Rose GJ. Mechanisms of long-interval selectivity in midbrain auditory neurons: roles of excitation, inhibition, and plasticity. *J Neurophysiol* 100: 3407–3416, 2008.
- Feldmeyer D, Lübke J, Sakmann B. Efficacy and connectivity of intracolumnar pairs of layer 2/3 pyramidal cells in the barrel cortex of juvenile rats. *J Physiol* 575: 583–602, 2006.
- Feldmeyer D, Lübke J, Silver RA, Sakmann B. Synaptic connections between layer 4 spiny neurone-layer 2/3 pyramidal cell pairs in juvenile rat barrel cortex: physiology and anatomy of interlaminar signalling within a cortical column. *J Physiol* 538: 803–822, 2002.
- Fino F, Yuste R. Dense inhibitory connectivity in neocortex. *Neuron* 69: 1188–1203, 2011.
- Forsythe ID, Westbrook GL. Slow excitatory postsynaptic currents mediated by *N*-methyl-D-aspartate receptors on cultured mouse central neurones. *J Physiol* 396: 515–533, 1988.
- Fortune ES, Rose GJ. Passive and active membrane properties contribute to the temporal filtering properties of midbrain neurons in vivo. *J Neurosci* 17: 3815–3825, 1997.
- Fortune ES, Rose GJ. Short-term synaptic plasticity as a temporal filter. *Trends Neurosci* 24: 381–385, 2001.
- Fortune ES, Rose GJ. Voltage-gated Na<sup>+</sup> channels enhance the temporal filtering properties of electrosensory neurons in the torus. *J Neurophysiol* 90: 924–929, 2003.
- Friedman MA, Hopkins CD. Neural substrates for species recognition in the time-coding electrosensory pathway of mormyrid electric fish. *J Neurosci* 18: 1171–1185, 1998.
- George AA, Lyons-Warren AM, Ma X, Carlson BA. A diversity of synaptic filters are created by temporal summation of excitation and inhibition. *J Neurosci* 31: 14721–14734, 2011.
- Gill T. On the West African genus *Hemichromis* and description of new species in the museums of the Academy and Smithsonian Institution. *Proc Natl Acad Sci Phila* 14: 134–139, 1862.
- Grillner SG, Markram H, De Schutter E, Silberberg G, LeBeau FE. Microcircuits in action—from CPGs to neocortex. *Trends Neurosci* 28: 525–533, 2005.
- Harnett MT, Makara JK, Spruston N, Kath WL, Magee JC. Synaptic amplification by dendritic spines enhances input cooperativity. *Nature* 491: 599–602, 2012.
- Hartline HK. Visual receptors and retinal interaction. *Science* 164: 270–278, 1969.
- Hopkins CD, Bass AH. Temporal coding of species recognition signals in an electric fish. *Science* 212: 85–87, 1981.
- Houweling AR, Brecht M. Behavioural report of single neuron stimulation in somatosensory cortex. *Nature* 451: 65–68, 2008.
- Kampa B, Letzkus J, Stuart G. Cortical feed-forward networks for binding different streams of sensory information. *Nat Neurosci* 9: 1472–1473, 2006.
- Khosravi-Hashemi N, Fortune ES, Chacron MJ. Coding movement direction by burst firing in electrosensory neurons. *J Neurophysiol* 106: 1954–1968, 2011.
- Klug A, Borst JG, Carlson BA, Kopp-Scheinpflug C, Klyachko VA, Xu-Friedman MA. How do short-term changes at synapses fine-tune information processing? *J Neurosci* 32: 14058–14063, 2012.
- Ko H, Hofer SB, Pichler B, Buchanan KA, Sjöström PJ, Mrsic-Flogel TD. Functional specificity of local synaptic connections in neocortical networks. *Nature* 473: 87–91, 2011.
- Kwan AC, Dan Y. Dissection of cortical microcircuits by single-neuron stimulation in vivo. *Curr Biol* 22: 1459–1467, 2012.
- Li CY, Poo MM, Dan Y. Burst spiking of a single cortical neuron modifies global brain state. *Science* 324: 643–646, 2009.
- Liu SJ, Lachamp P. The activation of excitatory glutamate receptors evokes a long-lasting increase in the release of GABA from cerebellar stellate cells. *J Neurosci* 26: 9332–9339, 2006.
- Lübke J, Markram H, Frotscher M, Sakmann B. Frequency and dendritic distribution of autapses established by layer 5 pyramidal neurons in the developing rat neocortex: comparison with synaptic innervation of adjacent neurons of the same class. *J Neurosci* 16: 3209–3218, 1996.
- Lyons-Warren AM, Hollmann M, Carlson BA. Sensory receptor diversity establishes a peripheral population code for stimulus duration at low intensities. *J Exp Biol* 215: 2586–2600, 2012.

- Markram H, Lübke J, Frotscher M, Roth A, Sakmann B.** Physiology and anatomy of synaptic connections between thick tufted pyramidal neurones in the developing rat neocortex. *J Physiol* 500: 409–440, 1997.
- Mathew SS, Hablitz JJ.** Presynaptic NMDA receptors mediate IPSC potentiation at GABAergic synapses in developing rat neocortex. *PLoS One* 6: e17311, 2011.
- McBain CJ, Mayer ML.** N-methyl-D-aspartic acid receptor structure and function. *Physiol Rev* 74: 723–760, 1994.
- Mishchenko Y, Hu T, Spacek J, Mendenhall J, Harris KM, Chklovskii DB.** Ultrastructural analysis of hippocampal neuropil from the connectomics perspective. *Neuron* 67: 1009–1020, 2010.
- Perin R, Berger TK, Markram H.** A synaptic organizing principle for cortical neuronal groups. *Proc Natl Acad Sci USA* 108: 5419–5424, 2011.
- Pollack GS.** Analysis of temporal patterns of communication signals. *Curr Opin Neurobiol* 11: 734–738, 2001.
- Poulet JF, Petersen CC.** Internal brain state regulates membrane potential synchrony in barrel cortex of behaving mice. *Nature* 454: 881–885, 2008.
- Reig R, Gallego R, Nowak L, Sanchez-Vives MV.** Impact of cortical network activity on short-term synaptic depression. *Cereb Cortex* 16: 688–695, 2006.
- Reyes A, Lujan R, Rozov A, Burnashev N, Somogyi P, Sakmann B.** Target-cell-specific facilitation and depression in neocortical circuits. *Nat Neurosci* 1: 279–285, 1998.
- Rose G.** A temporal-processing mechanism for all species? *Brain Behav Evol* 28: 134–144, 1986.
- Rose GJ, Fortune ES.** Mechanisms for generating temporal filters in the electrosensory system. *J Exp Biol* 202: 1281–1289, 1999.
- Rose GJ, Leary CJ, Edwards CJ.** Interval-counting neurons in the anuran auditory midbrain: factors underlying diversity of interval tuning. *J Comp Physiol A* 197: 97–108, 2011.
- Sachdev RN, Krause MR, Mazer JA.** Surround suppression and sparse coding in visual and barrel cortices. *Front Neural Circuits* 6: 1–14, 2012.
- Schluger JH, Hopkins CD.** Electric fish approach stationary signal sources by following electric current lines. *J Exp Biol* 130: 359–367, 1987.
- Shouval HZ, Bear MF, Cooper LN.** A unified model of NMDA receptor-dependent bidirectional synaptic plasticity. *Proc Natl Acad Sci USA* 99: 10831–10836, 2002.
- Song S, Sjöström P, Reigl M, Nelson S, Chklovskii DB.** Highly nonrandom features of synaptic connectivity in local cortical circuits. *PLoS Biol* 3: e68, 2005.
- Szuts TA, Fadeyev V, Kachiguine S, Sher A, Grivich MV, Agrochão M, Hottowy P, Dabrowski D, Lubenov EV, Siapas AG, Uchida N, Litke AM, Meister M.** A wireless multi-channel neural amplifier for freely moving animals. *Nat Neurosci* 14: 263–269, 2011.
- Takahashi N, Kitamura K, Matsuo N, Mayford M, Kano M, Matsuki N, Ikegaya Y.** Locally synchronized synaptic inputs. *Science* 335: 353–356, 2012.
- Thivierge JP, Marcus GF.** The topographic brain: from neural connectivity to cognition. *Trends Neurosci* 30: 251–259, 2007.
- Vandecasteele M, Glowinski J, Venance L.** Electrical synapses between dopaminergic neurons of the substantia nigra pars compacta. *J Neurosci* 25: 291–298, 2005.
- Vervaeke K, Lörincz A, Gleeson P, Farinella M, Nusser Z, Silver RA.** Rapid desynchronization of an electrically coupled interneuron network with sparse excitatory synaptic inputs. *Neuron* 67: 435–451, 2010.
- von der Emde G.** Active electrolocation of objects in weakly electric fish. *J Exp Biol* 202: 1205–1215, 1999.
- Wang Y, Barakat A, Zhou H.** Electrotonic coupling between pyramidal neurons in the neocortex. *PLoS One* 5: e10253, 2010.
- Wang Y, Gupta A, Toledo-Rodriguez M, Wu CZ, Markram H.** Anatomical, physiological, molecular and circuit properties of nest basket cells in the developing somatosensory cortex. *Cereb Cortex* 12: 395–410, 2002.
- Wong RY, Hopkins CD.** Electrical and behavioral courtship displays in the mormyrid fish *Brienomyrus brachyistius*. *J Exp Biol* 210: 2244–2252, 2007.
- Xu-Friedman MA, Hopkins CD.** Central mechanisms of temporal analysis in the knollenorgan pathway of mormyrid electric fish. *J Exp Biol* 202: 1311–1318, 1999.
- Yoshimura Y, Dantzker JLM, Callaway E.** Excitatory cortical networks form fine-scale functional networks. *Nature* 433: 868–873, 2005.
- Zucker RS, Regehr WG.** Short-term synaptic plasticity. *Annu Rev Physiol* 64: 355–405, 2002.